Clim. Past, 12, 1889–1905, 2016
www.clim-past.net/12/1889/2016/
doi:10.5194/cp-12-1889-2016

Climate of the Past
Open Access
EGU

On the spatial and temporal variability of ENSO precipitation and drought teleconnection in mainland Southeast Asia

Timo A. Räsänen[1], **Ville Lindgren**[1], **Joseph H. A. Guillaume**[1], **Brendan M. Buckley**[2], **and Matti Kummu**[1]

[1]Water & Development Research Group, Aalto University, Tietotie 1E, 02150 Espoo, Finland
[2]Tree Ring Laboratory, Lamont-Doherty Earth Observatory of Columbia University, 61 Route 9W, Palisades, NY, USA

Correspondence to: Timo A. Räsänen (timo.rasanen@aalto.fi)

Received: 14 October 2015 – Published in Clim. Past Discuss.: 10 November 2015
Accepted: 20 June 2016 – Published: 21 September 2016

Abstract. The variability of the hydroclimate over mainland Southeast Asia is strongly influenced by the El Niño–Southern Oscillation (ENSO), which has been linked to severe droughts and floods that profoundly influence human societies and ecosystems alike. Although the significance of ENSO is well understood, there are still limitations in the understanding of its effects on hydroclimate, particularly with regard to understanding the spatio-temporal characteristics and the long-term variation of its effects. Therefore we analysed the seasonal evolution and spatial variations in the effect of ENSO on precipitation over the period of 1980–2013 and the long-term variation in the ENSO teleconnection using tree-ring-derived Palmer drought severity indices (PDSIs) for the March–May season that span over the time period 1650–2004. The analyses provided an improved understanding of the seasonal evolution of the precipitation anomalies during ENSO events. The effects of ENSO were found to be most consistent and expressed over the largest areal extents during March–May of the year when the ENSO events decay. On a longer timescale, we found that ENSO has affected the region's March–May hydroclimate over the majority (95 %) of the 355-year study period and that during half (52 %) of the time ENSO caused a significant increase in hydroclimatic variability. The majority of the extremely wet and dry March–May seasons also occurred during ENSO events. However, considerable variability in ENSO's influence was revealed: the spatial pattern of precipitation anomalies varied between individual ENSO events, and the strength of ENSO's influence was found to vary through time. Given the high variability in ENSO teleconnection that we described and the limitations of the current understanding of the effects of ENSO, we suggest that the adaptation to ENSO-related extremes in hydroclimate over mainland Southeast Asia needs to recognise uncertainty as an inherent part of adaptation, must go beyond "predict and control", and should seek adaptation opportunities widely within society.

1 Introduction

Extremes or changes in the mean state of climate can result in great duress to societies, especially during periods of prolonged drought or flood. A well-known source of droughts and floods on a global scale is the ocean–atmosphere coupled phenomena El Niño–Southern Oscillation (ENSO) (Cane, 2005; Ward et al., 2014). ENSO is an evolving phenomenon (Trenberth and Shea, 1987), and it has become increasingly variable over recent decades (McGregor et al., 2013; Cai et al., 2014).

Over mainland Southeast Asia, henceforth MSEA, ENSO explains a large part of the inter-annual hydrological variability (Juneng and Tangang, 2005), and many of the recent severe droughts and floods occurred during ENSO events (see e.g. Räsänen and Kummu, 2013). Changes in hydroclimate variability is of great concern to the largely agrarian population of MSEA, as their livelihoods, economy, and food security are strongly dependent upon hydroclimatic conditions (MRC, 2010; Keskinen et al., 2010; ADB, 2016; Pech and Sunada, 2008). This dependency has triggered several studies that investigate the hydroclimatic variability and particularly the role of ENSO over MSEA.

Past research has shown that ENSO modulates precipitation and river flows over MSEA (Cook et al., 2012; Anchukaitis et al., 2016). Precipitation over MSEA is known to

decrease during warm-phase (El Niño) events and increase during cool-phase (La Niña) events (Juneng and Tangang, 2005; Singhrattna et al., 2005b; Räsänen and Kummu, 2013; Kripalani and Kulkarni, 1997). The effects of El Niño on precipitation have been reported to evolve over Southeast Asia from south to north during development and decay phases of the events and particularly affect the southern parts of MSEA during the spring when the events decay (Räsänen and Kummu, 2013; Juneng and Tangang, 2005). ENSO's correlation with precipitation is known to be strongest in southern MSEA, weakening towards the north, and there are indications of opposite correlation between southern and northern areas (Kiem et al., 2005; Räsänen and Kummu, 2013; Zhang et al., 2007). These studies have contributed to the understanding on the effects of ENSO on precipitation over MSEA, and they provide either a high-resolution view over a smaller area or a coarse-resolution view over a larger area, but they do not provide a high-resolution view over the entire MSEA and its largest river basins, particularly on seasonal scales.

ENSO-related hydroclimatic anomalies over MSEA are known to vary through time. In general, during periods when hydrological conditions are below (above) average the effects of El Niño (La Niña) on precipitation are more severe (Kripalani and Kulkarni, 1997). Precipitation analyses over Thailand show that the connection between precipitation and ENSO has become stronger in the post-1980 period (Singhrattna et al., 2005b). Variation in the relationship between ENSO and hydroclimate is also found in the river flows. The analyses of the Mekong River show a stronger relationship between ENSO and river flow before the 1940s and after the late 1970s (Räsänen and Kummu, 2013; Darby et al., 2013). The changes in the relationship between ENSO and hydroclimate are linked to changes in ENSO's connection to different monsoon components. MSEA lies between the Indian summer monsoon (ISM) and western North Pacific summer monsoon (WNPSM) regions, and since the late 1970s the relationship between ENSO and WNPSM has strengthened while the relationship between ENSO and ISM has weakened (Wang et al., 2008; Hsu et al., 2014). These studies have shown temporal variations in the effects of ENSO in MSEA, albeit only over the last 100 years or so.

Xu et al. (2013) reconstructed the multivariate ENSO index using stable isotopes of Oxygen (^{18}O) from cross-dated tree rings of the Vietnamese cypress (*Fokienia hodginsii*). Their results illustrate the long-term influence of ENSO over the region, identifying at least 121 El Niño and 130 La Niña events between the years of 1605 and 2002. Other hydrological reconstructions also suggest long-term connection between ENSO and the regional hydroclimate, and make an unequivocal linkage between severe droughts and El Niño events (Buckley et al., 2007, 2010, 2014; Sano et al., 2008). However, the studies focusing on the long-term ENSO teleconnection over MSEA did not investigate the temporal variation systematically.

Altogether, the body of research described above shows that the understanding of the linkage between ENSO and hydroclimate over MSEA has developed rapidly over recent years, but gaps exist, and there is a need to draw a more coherent picture. In this paper we focus on a research need consisting of combined analysis of three aspects: (1) high-spatial-resolution understanding of the seasonal evolution of correlation patterns between ENSO and precipitation, covering MSEA and its largest river basins; (2) spatial variation in precipitation anomaly patterns between individual ENSO events over MSEA; and (3) long-term temporal variation and stationarity of the ENSO teleconnection over MSEA. Advancing the knowledge of these three aspects would improve the scientific understanding of ENSO teleconnection and thus provide valuable information for adaptation to ENSO-related hydrological variability over MSEA and its largest river basins.

We therefore aim to analyse the instrumental and proxy records of hydroclimate over the region (Fig. 1). First we analyse instrumental records of precipitation over the period of 1980–2013 in order to investigate the seasonal evolution and spatial variation in the effect of ENSO on precipitation over MSEA, and second we analyse tree-ring-based proxy Palmer drought severity index data (PDSI; see Palmer, 1965) for the March–May season from two areas in MSEA that cover the time period of 1650–2004 to investigate the long-term variations in ENSO teleconnection. The methodology of using both precipitation and proxy PDSI data together aims to provide a more coherent view of the spatial and temporal variability in the effects of ENSO.

2 Methodology

The spatial and temporal analysis of ENSO's influence on hydroclimate is divided into two parts: analysis of seasonal precipitation over MSEA for the period 1980–2013, and analysis of proxy PDSI (for PDSI see Palmer, 1965) for the March–May season from two locations in MSEA over the period of 1650–2004.

The precipitation analysis aimed to improve our understanding of the spatial and temporal patterns of ENSO-related precipitation anomalies as well as our understanding of the strength of the relationship between ENSO and hydroclimate over the two proxy PDSI regions. The precipitation was analysed using precipitation data from the Global Precipitation and Climatology Centre (GPCC) (Schneider et al., 2015), the multivariate ENSO index (MEI) (Wolter and Timlin, 1993, 1998), and correlation analyses.

The analyses of proxy PDSI data aimed to improve the understanding of how the ENSO–hydroclimate teleconnection over MSEA has varied through time. Our analyses focus on the months of March–May, which span the transition period from dry to wet season, when the monsoon precipitation gradually starts (Adamson and Bird, 2010). March–May is

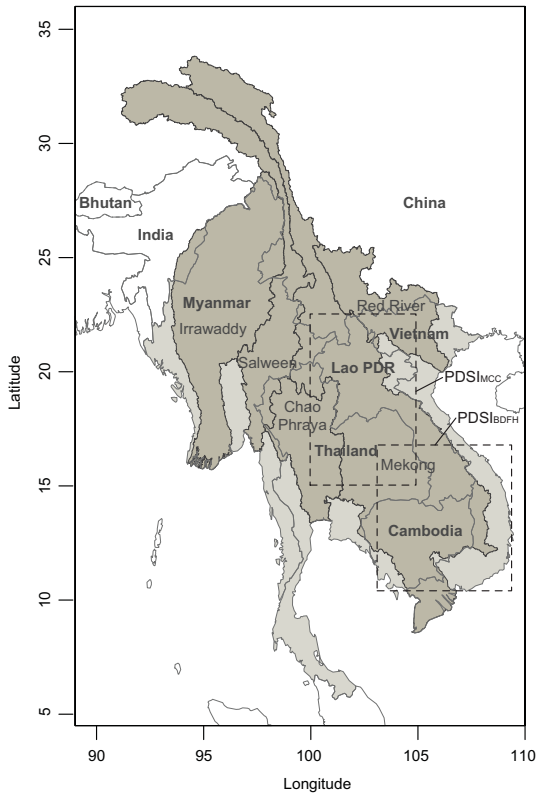

Figure 1. Map of the study area: mainland Southeast Asia. The spatial variability of ENSO's influence was analysed using annual precipitation data over the period of 1980–2013 with a focus on the area covering Myanmar, Thailand, Lao PDR, Vietnam, and Cambodia and the largest river basins: the Irrawaddy, Salween, Chao Phraya, Mekong, and Red rivers. The temporal variability of ENSO's influence was analysed using proxy Palmer drought severity index (PDSI) data for the March–May season over the period of 1650–2004 with a focus on two regions shown in the figure with rectangles denoting the $PDSI_{MCC}$ and $PDSI_{BDFH}$ reconstruction fields of Sano et al. (2008) and Buckley et al. (2010), respectively.

also the beginning of the sowing season of rainfed rice in many areas (see e.g. Sawano et al., 2008), and the conditions of the early monsoon affect the transplanting of rice and thus the productivity of the crops (Fukai et al., 1998). The analyses of proxy PDSI data were based on two tree ring reconstructions from southern and northern Vietnam (Sano et al., 2008; Buckley et al., 2010; Cook et al., 2010), the unified ENSO proxy (McGregor et al., 2010), and correlation and wavelet methods (e.g. Torrence and Compo, 1998). In addition we analysed the co-occurrence of extremely dry and wet March–May seasons with ENSO events.

2.1 Precipitation analysis 1980–2013

The seasonal precipitation analysis was based on GPCC v.7 data (Schneider et al., 2015), which is an observation-based gridded climatological data set with temporal coverage of 1901–2013 and spatial resolution of 0.5° (ca. 55 km at the Equator). The analysis of precipitation was done on a seasonal basis: June–July–August (JJA), September–October–November (SON), December–January–February (DJF), and March–April–May (MAM). The analysis was limited to the post-1980 period as previous research (Räsänen and Kummu, 2013) has reported that there are considerably fewer weather stations in the pre-1980 period. In addition, the post-1980 period exhibits a stronger relationship between ENSO and hydrology (Räsänen and Kummu, 2013; Räsänen et al., 2013; Singhrattna et al., 2005b). The data sets used for the precipitation analysis are summarised in Table 1.

We also considered precipitation data from the Climate Research Unit (CRU TS v.3.21; Harris et al., 2014) and from Asian Precipitation – Highly Resolved Observational Data Integration Towards Evaluation (APHRODITE; Yatagai et al., 2009, 2012) precipitation data for the analyses, but comparisons suggested that GPCC v.7 was the most suitable. CRU TS v.3.21 had major gaps in stations in the region of Myanmar, and APHRODITE covers only a time period until 2007 and therefore does not capture the most recent influential ENSO events. The comparison of GPCC v.7 and APHRODITE over their common period provided very similar results.

First, the seasonal evolution of ENSO-related precipitation patterns was analysed. ENSO events are generally 2-year phenomena that start to develop in spring, mature late in the same year or early the next year, and decay in the following summer. Therefore the precipitation was aggregated into JJA(0), SON(0), DJF(0/1), MAM(1), JJA(1), and SON(1) seasonal sums and correlated with the time series of the January–February–March value of MEI (NOAA, 2015) from the second year of each ENSO event (MEI_{JFM}). MEI is a monthly index that describes the phases of ENSO, and it is calculated from six variables from the tropical Pacific Ocean: sea level pressure, zonal and meridional components of the surface wind, sea surface temperature, surface air temperature, and total cloudiness fraction of the sky (NOAA, 2015). January–February–March (JFM) forms part of the peaking period of ENSO events, and thus the MEI index values from these months represent the occurrence and strength of individual ENSO events (see e.g. Räsänen and Kummu, 2013; Singhrattna et al., 2005a). The notations "0" and "1" in the names of the seasons denote the first year (i.e. developing year) and the second year (i.e. decaying year) of an ENSO event, respectively. On a few occasions the ENSO event lasted 3 years, and this third year of ENSO event was denoted with "2". Pearson's correlation was used to correlate seasonal precipitation and MEI_{JFM} at grid level, resulting in seasonal correlation maps.

Second, we analysed the seasonal precipitation anomalies for each ENSO event and for each season over MSEA. Anomalies were calculated as deviations from the 1980–2013 average precipitation and reported as percentages. This yielded seasonal precipitation anomaly maps of all El Niño

Table 1. Description of the data sets used in the analyses of this study.

Analysis	Name	Data description	Source
Precipitation analysis 1980–2013	Precipitation	GPCC v.7. Observation-based monthly gridded climatological data set with temporal coverage of 1901–2013 and spatial resolution of 0.5° (ca. 55 km at the Equator).	Schneider et al. (2015)
	MEI_{JFM}	Multivariate ENSO index. Bi-monthly index based on sea level pressure, zonal and meridional components of the surface wind, sea surface temperature, surface air temperature, and cloudiness data. JFM refers to index months of January–March that were used in this study.	Wolter and Timlin (1993) Wolter and Timlin (1998)
Proxy PDSI analysis 1650–2004	$PDSI_{BDFH}$	Tree-ring-based Palmer drought severity index reconstruction from northern Vietnam describing March–May monsoon conditions with temporal coverage of 1250–2008.	Buckley et al. (2010)
	$PDSI_{MCC}$	Tree-ring-based Palmer drought severity index reconstruction from southern Vietnam describing March–May monsoon conditions with temporal coverage of 1470–2004.	Sano et al. (2008)
	$ENSO_{UEP}$	Unified ENSO proxy. Proxy index based on the 10 most commonly used ENSO proxies with temporal coverage of 1650–1977. In this study the unified ENSO proxy was extended to cover the time period up to 2004 using MEI, similarly to McGregor et al. (2010).	McGregor et al. (2010)
	Multi-proxy ENSO event reconstruction	Multi-proxy ENSO event reconstruction. An annual record of El Niño and La Niña events and their strength with temporal coverage of 1525–2002.	Gergis and Fowler (2009)

and La Niña events for the period of 1980–2013. In addition, we analysed the precipitation anomalies in more detail at the locations of proxy PDSI data in order to understand how strongly the hydroclimate at those locations is related to ENSO. This helps to assess how well the PDSI proxies are suited for analysing long-term ENSO teleconnection.

2.2 Proxy PDSI analysis 1650–2004

The temporal variability of ENSO's teleconnection to MSEA was analysed using two tree-ring-based PDSI reconstructions developed by Sano et al. (2008) and Buckley et al. (2010), for northern and southern Vietnam, respectively. These two reconstructions marked the first two successful calibration-verification model schemes from tropical tree rings, both from the long-lived Vietnamese cypress (*Fokienia hodginsii*) of the family Cupressaceae, regressed against the PDSI data set of Dai et al. (2004). In both cases the season of reconstruction was the 3-month monsoon onset period of March–May, which is strongly influenced by the ENSO phenomenon (see Buckley et al., 2010, 2014). Together these two reconstructions cover a large portion of MSEA over Vietnam, Laos, Thailand, and Cambodia. The PDSI reconstructions are referred to hereafter as $PDSI_{BDFH}$ (Buckley et al., 2010) and $PDSI_{MCC}$ (Sano et al., 2008) based on the names of the study areas in the original publications. The data sets used in the proxy PDSI analysis are summarised in Table 1.

We used the unified ENSO proxy (UEP), an index based on the 10 most commonly used ENSO proxies that was published by McGregor et al. (2010), to describe ENSO behaviour over the period 1650–2005. The original UEP is annual data and covers the time period from 1650 to 1977. We extended the UEP up to the year 2004 by using MEI in order to match the time period of the PDSI data. To do so, we scaled the UEP variance to match the variance of MEI ($UEP \times \sigma_{MEI}/\sigma_{UEP}$) over the common period 1951–1977 for the annual average (July–June) of the two data sets, similarly to McGregor et al. (2010). The correlation between UEP and MEI over their common period is 0.81 ($p < 0.001$). The extended UEP is referred to hereafter as $ENSO_{UEP}$.

The $PDSI_{BDFH}$, $PDSI_{MCC}$, $ENSO_{UEP}$, and their relationships were analysed using moving-window correlation and

wavelet methods (see e.g. Torrence and Compo, 1998; Grinsted et al., 2004). Moving window correlations were used to examine the temporal variation in the correlation between $ENSO_{UEP}$ and PDSI data. Pearson's correlation was used with a window width of 21 years, which was deemed sufficiently insensitive to short-term variation. The statistical significance of correlations in each moving window was tested using the one-tailed Student's t test with 5 % significance level.

The applied wavelet methods included the computation of the wavelet power spectrum of a single time series, as well as the cross-wavelet power spectrum and wavelet coherence spectrum of two time series together. The computations were done using the WaveletComp R package developed by Rösch and Schmidbauer (2014). The wavelet power spectrum shows the time series in time-frequency space, which allows the examination of variations and their power with respect to their frequency and occurrence in time, while the cross-wavelet power spectrum shows where the variations of two time series have high common power in the time-frequency space. The wavelet coherence spectrum shows the coherence (i.e. localised correlation) between the two time series in time-frequency space, while the cross-wavelet power spectrum and the wavelet coherence spectrum also show the phase relationship between the two time series. In the case of correlated phenomena, the phase relationship is expected to be consistent in time. A more complete treatment of the wavelet methods can be found in Torrence and Compo (1998) and Grinsted et al. (2004).

The wavelet methods were used to identify temporal variability in the strength of ENSO's influence on hydroclimate over MSEA. Two categories were used for this identification: (i) primary ENSO-related variance and (ii) secondary ENSO-related variance in the hydroclimate of MSEA. These periods were defined according to regions in wavelet power, cross-wavelet power, and coherence spectrum that were overlapping in time-frequency space and fulfilled specific criteria. The specific criteria are explained in detail in Table 2. The major difference between the two categories is that in the former the increase of the wavelet power is statistically significant. Non-significant ENSO-related increases in wavelet power are also analysed as they reveal periods that still do have statistical relationship between ENSO and hydroclimate and provide an indication of the variations in the strength of ENSO teleconnection over MSEA. The wavelet analyses focused on periodicities from 2 to 10 years as they represent the frequencies of inter-annual ENSO variability. The statistical significance of the wavelet power and coherency was tested against white noise at the 5 % significance level.

In addition to wavelet analysis, we employed a variance analysis of the PDSI with an 11-year moving window in order to identify periods with high inter-annual variability in the time domain. This process also enabled us to see how well these periods correspond with the high-variability periods identified from wavelet analysis. We chose 11 years in order to capture the band of inter-annual variability without the decadal variability.

The co-occurrence of extremely dry and wet years with ENSO events was based on the Gergis and Fowler (2009) multi-proxy ENSO event reconstruction over the period of 1525–2002. The extreme years were defined from PDSI data using 5th and 95th percentiles, which meant that 10 % of all years of PDSI data were defined as extreme. The co-occurrence of extreme years with warm- and cool-phase ENSO events was then identified by comparing the multi-proxy ENSO event reconstruction and extreme PDSI values.

3 Results

3.1 ENSO and precipitation 1980–2013

The seasonal correlation analysis of precipitation and MEI_{JFM} shows different spatial correlation patterns for each season as shown in Fig. 2. The most distinctive feature of the seasonal correlations is the evolution of areas of statistically significant negative correlation from SON(0) to JJA(1) ($r < -0.339$, 5 % significance level) in the region of Thailand, Cambodia, Vietnam, and southern Myanmar, and the wide area of statistically significant positive correlation ($r > 0.339$, 5 % significance level) in DJF(0/1) in the region of China, northern Myanmar, northern Vietnam, and the Lao People's Democratic Republic (PDR). The negative (positive) correlation corresponds to reduced (increased) precipitation during El Niño and increased (reduced) precipitation during La Niña.

Taking a closer look at these patterns, the negative correlations are observed during SON(0) in the southern coastal regions of MSEA in the west in Thailand and Myanmar and in the east in southern Vietnam and Cambodia. In DJF(0/1) the areas of negative correlation are pushed further south by areas of positive correlations. In MAM(1) the negative correlations are widespread and cover most of the study area, except northern Myanmar and parts of China. In JJA(1) the areas of negative correlations are observed mainly in western Thailand and in southern Myanmar, and in SON(1) the negative correlations have more or less disappeared. Another interesting feature is the statistically significant positive correlation during the JJA(0) season in southern Myanmar, southern Lao PDR, and northern Cambodia, separated by an area of negative correlation in Thailand.

The analysis of precipitation anomalies shows spatially varying anomaly patterns between ENSO events. This can be observed in Fig. 3, which shows the MAM(1) precipitation anomalies of eight El Niño and four La Niña events during the period of 1980–2013 (see also Figs. S1 and S2 in the Supplement, which show precipitation anomalies for all seasons for the same El Niño and La Niña events as in Fig. 3).

In the case of the El Niño events of 1982–1983, 1986–1987, 1991–1992, 1994–1995, 1997–1998, and 2009–2010 (Fig. 3a–h), the MAM(1) precipitation anomalies are widely

Table 2. The identification criteria for periods with ENSO-related variance in March–May hydroclimate. Two types of variance periods were identified from unified ENSO proxy and PDSI proxy data: primary ENSO-related variance and secondary ENSO-related variance in the hydroclimate. These periods were defined according to regions in wavelet power spectrum (WP), cross-wavelet power (CWP), and coherence spectrum (WC) that were overlapping in time-frequency space and fulfilled the criteria in the table. Variance period refers to period when ENSO had increased influence on the March–May hydroclimate in mainland Southeast Asia.

Identification criteria	Secondary ENSO-related variance in the hydroclimate	Primary ENSO-related variance in the hydroclimate
WP of PDSI: increase in the power	√	√ Statistically significant ($p<0.05$)
WP of $ENSO_{UEP}$: increase in the power	√	√
CWP: increase in the common power	√	√ Statistically significant ($p<0.05$)
WC: statistically significant coherence ($p<0.05$)	√	√
CWP and WC: phase arrows suggest consistent phase lock	√	√

negative in large parts of the study area. During the El Niño event of 2002–2003 the negative precipitation anomalies are smaller in magnitude, and positive anomalies are observed in some regions, for example in southern Myanmar and at the border between southern Lao PDR and western Thailand. During the El Niño event of 2006–2007 the precipitation anomalies are mainly positive and thus inconsistent with other El Niño events.

In the case of La Niña events there is greater inconsistency in spatial patterns of MAM(1) precipitation anomalies than in the case of El Niño. During the 1998–1999 La Niña event, the MAM(1) precipitation anomalies are largely positive and cover Thailand, Cambodia, southern Lao PDR, southern Vietnam, and large parts of Myanmar. During the 1988–1989 event, the positive precipitation anomalies are confined to the eastern part of the study area in Vietnam, in 2007–2008 the precipitation anomalies are smaller but more widespread and can be seen particularly in Cambodia and eastern Thailand, and in the 2010–2011 event the positive precipitation anomalies are mainly in Myanmar and in western Thailand.

The time series analysis of MAM(1) precipitation for the areas of $PDSI_{BDFH}$ and $PDSI_{MCC}$ (see locations in Fig. 3) shows high correlation between precipitation and MEI_{JFM} and high consistency in the direction of precipitation anomalies during El Niño and La Niña events, as shown in Table 3. The Pearson's and Kendall's correlations for MAM(1) precipitation and MEI_{JFM} in the area of $PDSI_{BDFH}$ are -0.79 ($p<0.001$) and -0.64 ($p<0.001$), respectively. Similarly for the area of $PDSI_{MCC}$, the Pearson's and Kendall's correlations for MAM(1) precipitation and MEI_{JFM} are -0.69 ($p<0.001$) and -0.5 ($p<0.001$), respectively.

During MAM(1+2) of El Niño events, the precipitation anomalies were negative for the $PDSI_{BDFH}$ area in 80 % of the events and for the $PDSI_{MCC}$ area in 70 % of the events (Table 3). During MAM(1+2) of La Niña events the precipitation anomalies for the $PDSI_{BDFH}$ and $PDSI_{MCC}$ areas were positive in 100 % of the events (Table 3). The strong El Niño events stand out in the magnitude of precipitation anomalies: the precipitation anomalies during the second and third years are on average -32 and -24 %, varying in the ranges (-41, -14 %) and (-50, -1 %) for the areas of $PDSI_{BDFH}$ and $PDSI_{MCC}$, respectively.

3.2 ENSO and proxy PDSI 1650–2004

The precipitation analyses provided a good understanding of the hydroclimate and its relationship to ENSO in the areas of $PDSI_{BDFH}$ and $PDSI_{MCC}$. The $PDSI_{BDFH}$ and $PDSI_{MCC}$ correspond to areas affected by ENSO. In particular, the hydroclimate of the MAM season, which the PDSI data also describe, showed high correlation with ENSO (see Fig. 2d). Therefore, $PDSI_{BDFH}$ and $PDSI_{MCC}$ are considered as good proxies for analysing the long-term ENSO teleconnection over MSEA.

The correlation analysis between $ENSO_{UEP}$ and $PDSI_{BDFH}$, and $ENSO_{UEP}$ and $PDSI_{MCC}$ with moving windows revealed that the correlations vary in time and also differ between $PDSI_{BDFH}$ and $PDSI_{MCC}$ (Fig. 4). Statistically significant negative correlations ($p<0.05$) can be observed for $PDSI_{BDFH}$ approximately during 93 %, and for $PDSI_{MCC}$ approximately during 67 %, of the study period. The longest period of no statistically significant correlation was observed for $PDSI_{MCC}$ during 1885–1948, which interestingly coincides with the period of highest correlation for $PDSI_{BDFH}$. The most recent period of statistically significant correlation started for both $PDSI_{BDFH}$ and $PDSI_{MCC}$ around the mid-20th century. In the early 19th century the correlation with $PDSI_{MCC}$ changes into a strong positive relationship. The periods with statistically significant correlation between PDSI data and $ENSO_{UEP}$ are listed in Table 4.

The wavelet analyses show a connection between ENSO and the hydroclimate of the region throughout the study period (Figs. 5–6). The connection can be observed as a relatively consistent temporal distribution of statistically significant areas in the wavelet coherence spectrum of $ENSO_{UEP}$ and $PDSI_{BDFH}$ (Fig. 5d) and $ENSO_{UEP}$ and $PDSI_{MCC}$

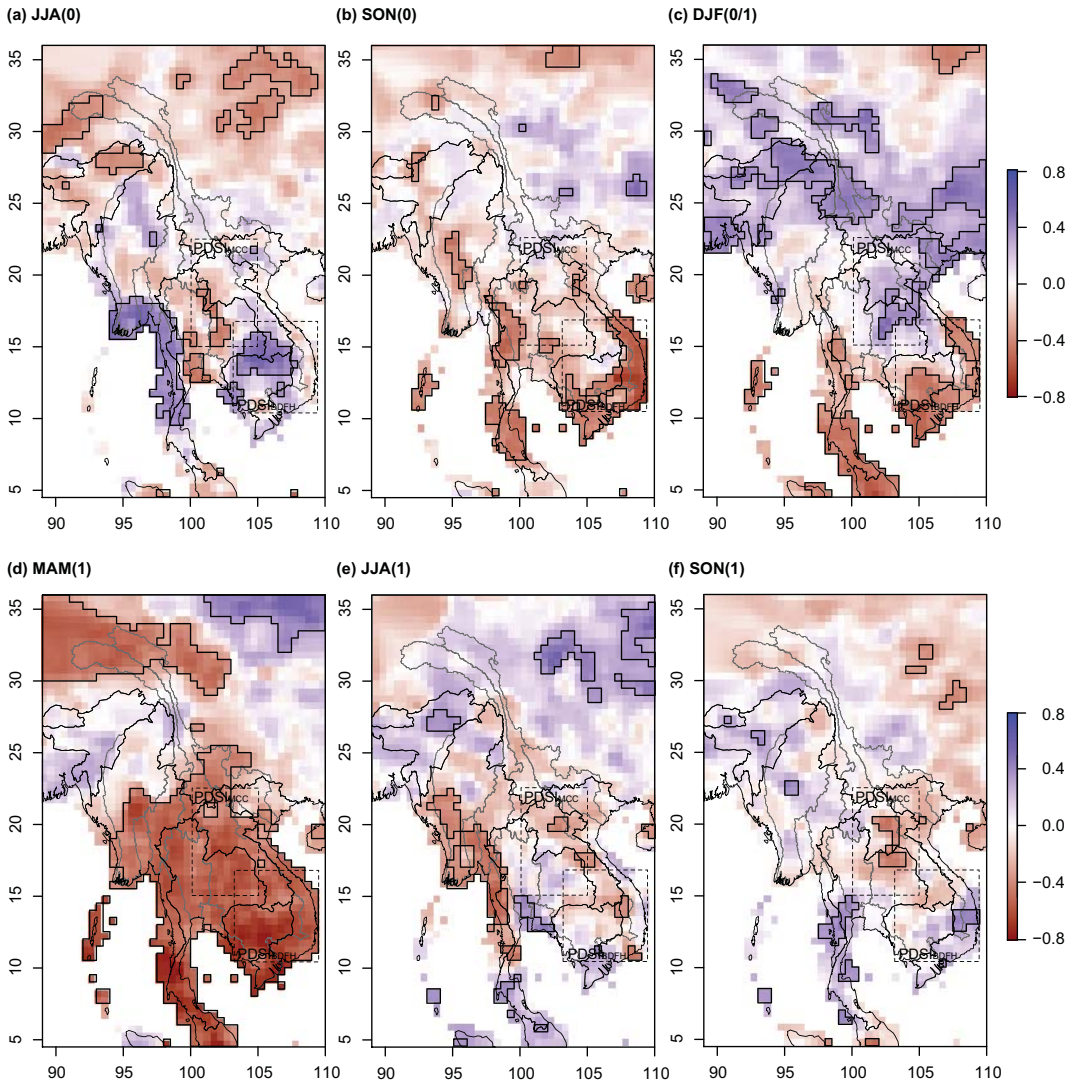

Figure 2. Map of correlation of January–February–March values of multivariate ENSO index (MEI_{JFM}) and seasonal precipitation over the period of 1980–2013: **(a)** June–July–August (JJA (0)), **(b)** September–October–November (SON(0)), **(c)** December–January–February (DJF(0/1)), **(d)** March–April–May (MAM(1)), **(e)** June–July–August (JJA (1)), and **(f)** September–October–November (SON(1)). "0" denotes the first (i.e. developing) year, and "1" denotes the second (i.e. decaying) year of ENSO events. Black lines delimit areas of statistically significant correlation ($|r| > 0.339$, 5 % significance level).

(Fig. 6d). However, there are periods when there is no statistically significant coherence and the phase arrows point in inconsistent directions, for example from the 1760s to the late 1770s, suggesting no connection between ENSO and the hydroclimate.

The wavelet analyses of $PDSI_{BDFH}$ in Fig. 5 show seven periods with primary ENSO-related variance and four periods with secondary ENSO-related variance in the hydroclimate. The periods with primary ENSO-related variance coincide also with the overall increase in the variance as shown by the moving-window analysis in Fig. 5b. For example, three periods with high variance are identified, and these coincide with the periods of 1735–1750, 1871–1899, and 1960–1980 with primary ENSO-related variance (Fig. 5). In $PDSI_{BDFH}$ there are also three periods with significant increase in wavelet power that could not be associated with $ENSO_{UEP}$ (Fig. 5b). Thus in the region of $PDSI_{BDFH}$, 7 out of 10 periods with statistically significant increase in wavelet power can be associated with ENSO. The identified periods with primary and secondary ENSO-related variance in $PDSI_{BDFH}$ are listed in Table 4.

The wavelet analyses of $PDSI_{MCC}$ show two periods with primary ENSO-related variance and 10 periods with secondary ENSO-related variance in the hydroclimate (Fig. 6; Table 4). Many of these periods coincide with the general increase in the variance as shown by the moving-window

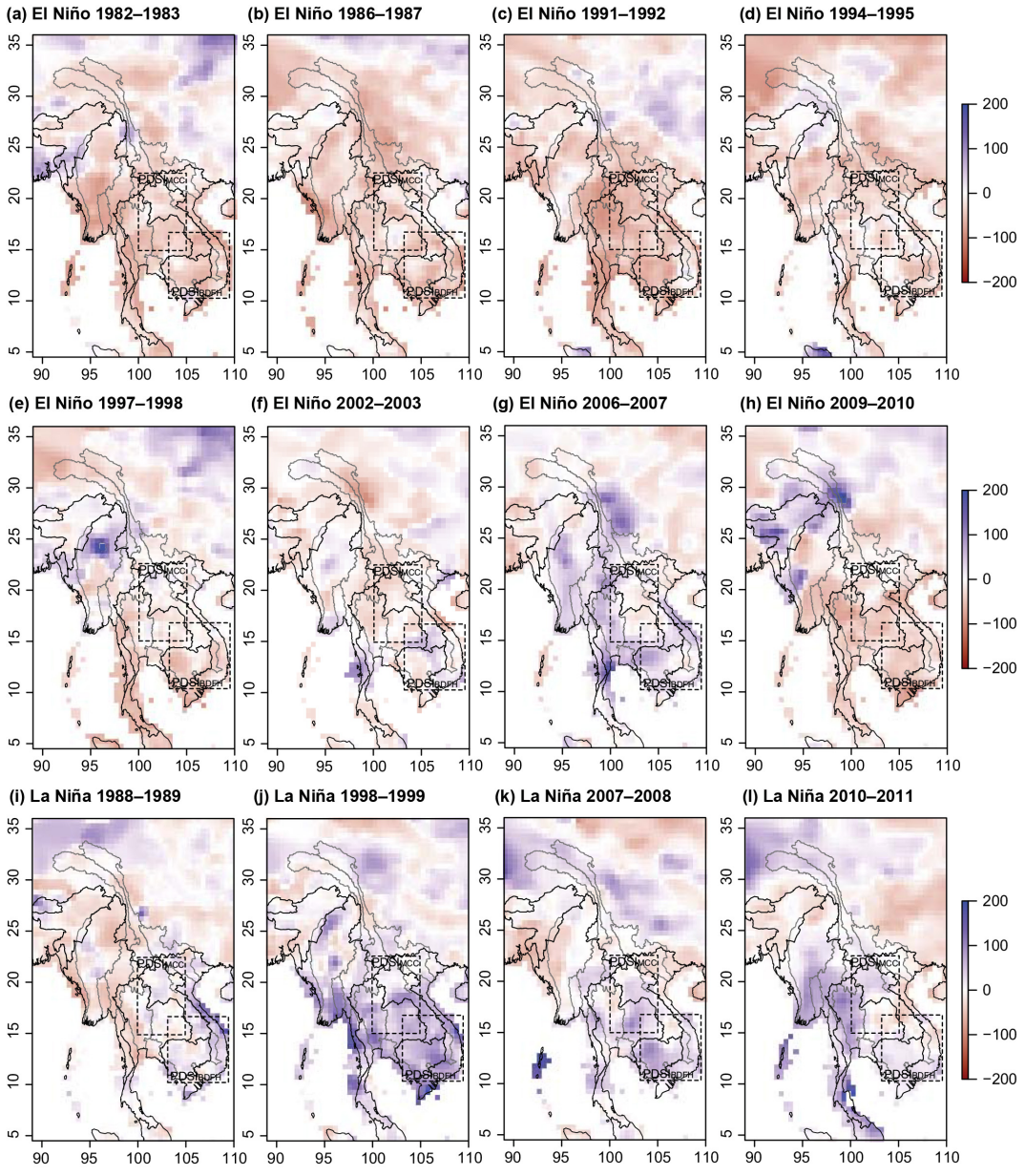

Figure 3. March–May precipitation anomalies (%) during the second year (MAM(1)) of **(a–h)** eight El Niño and **(i–j)** four La Niña events.

variance in Fig. 6b, for example in 1703–1745, 1829–1842, and 1949–1958. Statistically significant increase in wavelet power of $PDSI_{MCC}$ can be observed also during the first half of the 19th century (Fig. 6b), but its association with $ENSO_{UEP}$ is unclear. During this period both $ENSO_{UEP}$ and $PDSI_{MCC}$ show increase in wavelet power (Fig. 6a–b) and statistically significant coherence (Fig. 6d), but the phase arrows are pointing opposite to the general direction. The change in the direction of correlation was observed also in the analysis with moving-window correlation in Fig. 4. The identified periods with primary and secondary ENSO-related variance in $PDSI_{MCC}$ are listed in Table 4.

The wavelet analyses also reveal that increased variance in ENSO does not always result in increased hydroclimatic variance over MSEA. For example, the statistically significant increases in wavelet power of $ENSO_{UEP}$ in 1784–1795 (periodicities of about 5 and 8 years), 1901–1906 (periodicity of around 3 years), 1940–1955 (periodicities of about 4 and 6 years), and 1980–1989 (periodicity of 3–6 years) did not result in increase in wavelet power for $PDSI_{BDFH}$ (Fig. 5b). Similarly, the significant increases in wavelet power of $ENSO_{UEP}$ in 1784–1795 (periodicity of around 8 years) and 1915–1921 and 1981–1989 (periodicity of around 5 years) (Fig. 5a) did not result in increase in wavelet power

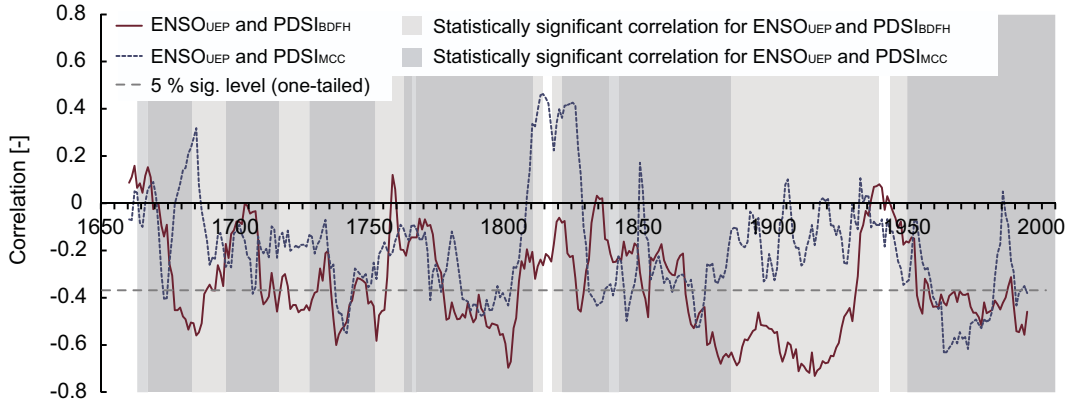

Figure 4. Correlations between $ENSO_{UEP}$ and $PDSI_{BDFH}$ and $ENSO_{UEP}$ and $PDSI_{MCC}$ using a 21-year moving window over the period of 1650–2004. PDSI data describe the hydroclimate of the March–May season.

for $PDSI_{MCC}$ (Fig. 6b). This suggests non-stationarity in the relationship between ENSO and hydroclimate over MSEA.

The analysis of extreme PDSI values in Figs. 5e and 6e shows that the majority of the most-extreme dry and wet MAM seasons occurred during ENSO events, particularly in the region of $PDSI_{BDFH}$. Altogether 18 years were defined with extremely dry and 18 years with extremely wet MAM seasons in $PDSI_{BDFH}$ and $PDSI_{MCC}$ using 5th and 95th percentiles. In the case of $PDSI_{BDFH}$, 13 (72 %) extremely dry MAM seasons occurred during El Niño events, and 13 (72 %) extremely wet MAM seasons occurred during La Niña events. For $PDSI_{MCC}$, the respective figures are 6 (33 %) extremely dry MAM seasons that occurred during El Niño events and 10 (56 %) extremely wet MAM seasons that occurred during La Niña events. This indicates in general that in the region of $PDSI_{BDFH}$ both extremely dry and wet MAM seasons tend to co-occur more often with ENSO events than in the region of $PDSI_{MCC}$.

When the results of the moving-window correlation analyses and the wavelet analyses of both $PDSI_{BDFH}$ and $PDSI_{MCC}$ are examined together, a more coherent picture can be drawn of ENSO's influence over MSEA (Fig. 7 and Table 4). There is evidence of ENSO signal in the hydroclimate of the MAM season over MSEA approximately 96 % of the time over the 355-year study period, but the strength of this ENSO signal varies across time and space. The wavelet analyses suggest that approximately 52 % of the study period can be classified as experiencing primary ENSO-related variance, while 17 % experiences secondary ENSO-related variance. The periods with ENSO-related variance in $PDSI_{BDFH}$ and $PDSI_{MCC}$ overlap each other relatively well, but there are also differences in the strength, timing, and duration.

4 Discussion

The research approach used, based on a combination of precipitation data and proxy PDSI data derived from tree ring records, provides a more uniform and coherent picture of the spatio-temporal effects of ENSO over MSEA and its largest river basins. The analysis of precipitation data showed how the precipitation anomalies evolve in time during ENSO events and how they vary in space between individual ENSO events. The analysis of proxy PDSI data in turn showed not only how the effects of ENSO have varied for the monsoon transition period (March–May) over a longer timescale but also how the effects have varied spatially between northern and southern areas of MSEA. In the following sections we further discuss important aspects of the methodology, state our contributions and compare our findings with past research, and suggest directions for future work as well as for adaptation to ENSO-related hydroclimatic anomalies.

4.1 On the methodology

The analysis of the long-term ENSO-hydroclimate relationship using two methods (moving-window correlation and wavelets) and two hydroclimate proxies derived from tree rings ($PDSI_{BDFH}$ and $PDSI_{MCC}$) was found to be a useful approach. The two methods and two hydrological proxies revealed aspects of this relationship that neither of the methods or data could have achieved alone. For example, wavelet methods revealed a statistical relationship between ENSO and hydroclimate, whereas the moving-window correlations did not (see e.g. Fig. 7). The two hydrological proxies complemented each other by capturing the spatially varying effects of ENSO and thus provided a more complete picture of the relationship between ENSO and hydroclimate.

However, there are certain limitations in the above approach in providing exact years for the periods with connection between ENSO and hydroclimate. First, the proxy PDSI analyses focused only on the MAM season. However, this season is deemed to be appropriate for detecting an ENSO signal over MSEA, as our analyses revealed that the correlation between ENSO and precipitation over MSEA was strongest and statistically significant over the largest area of

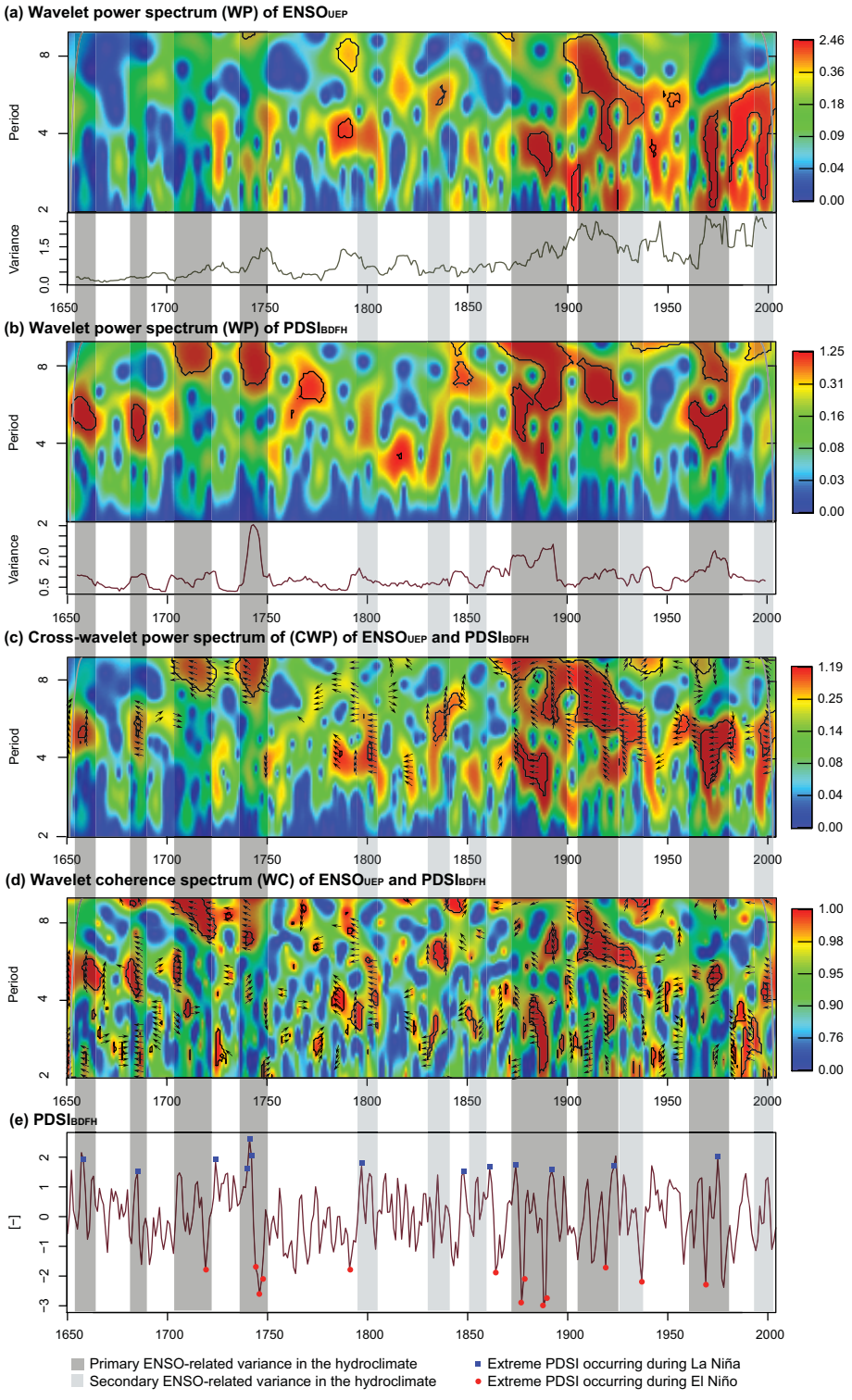

Figure 5. Wavelet analysis of ENSO and $PDSI_{BDFH}$ over the period 1650–2004. Wavelet power spectrum of **(a)** $ENSO_{UEP}$ and **(b)** $PDSI_{BDFH}$, **(c)** cross-wavelet power spectrum and **(d)** wavelet coherence spectrum of $ENSO_{UEP}$ and $PDSI_{BDFH}$, and **(e)** time series of $PDSI_{BDFH}$. Tiles **(a)** and **(b)** also show total variances of time series calculated with a moving window of 21 years. The dark grey columns indicate periods with primary ENSO-related variance, and the light grey columns indicate periods with secondary ENSO-related variance in $PDSI_{BDFH}$ (see definitions in Table 2). Tile E also shows extreme PDSI values that occurred during ENSO events. Extreme values were defined from PDSI data as 5th and 95th percentiles. PDSI data describe the hydroclimate of the March–May season.

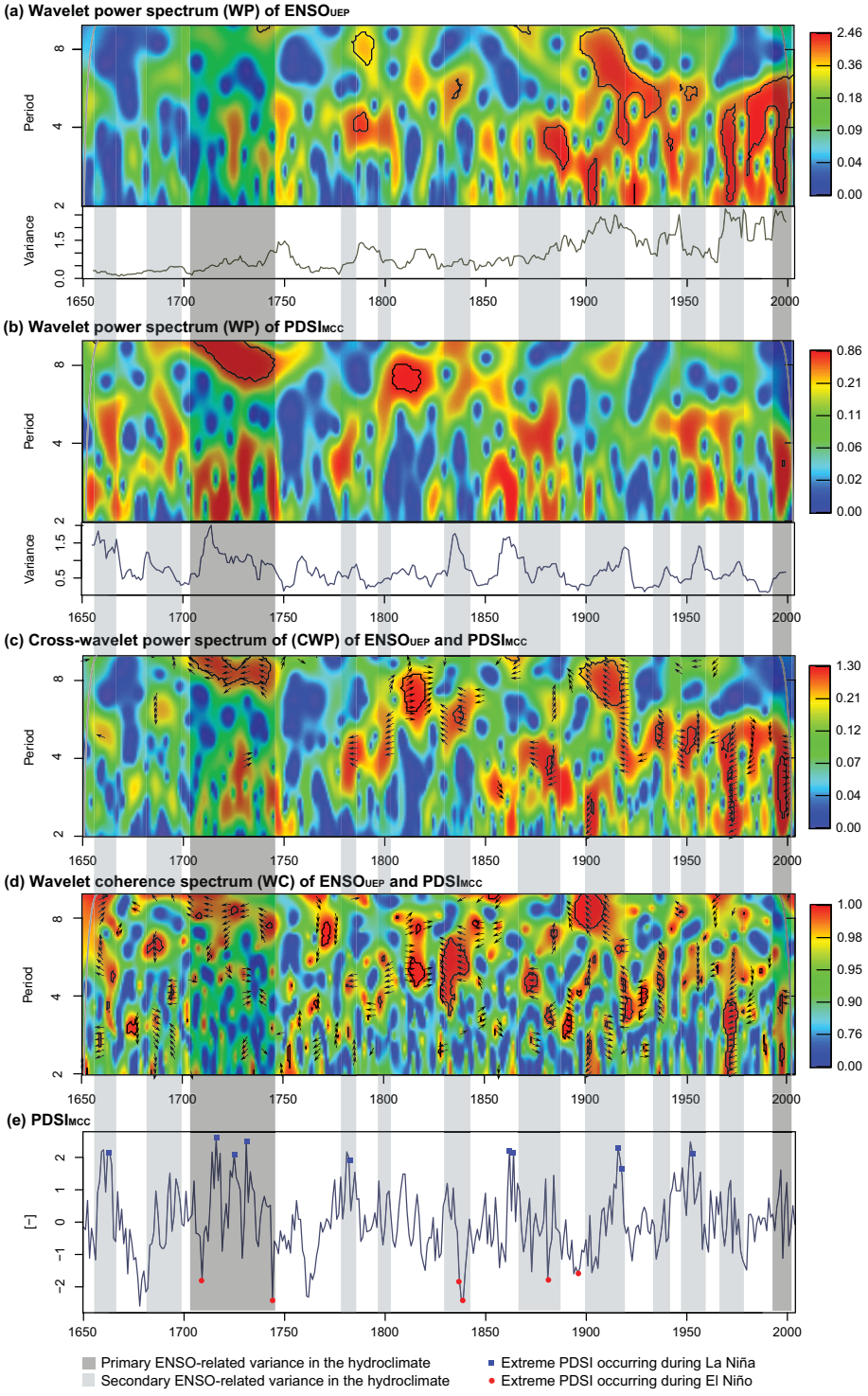

Figure 6. Wavelet analysis of ENSO and $PDSI_{MCC}$ over the period 1650–2004. Wavelet power spectrum of **(a)** $ENSO_{UEP}$ and **(b)** $PDSI_{MCC}$, **(c)** cross-wavelet power spectrum and **(d)** wavelet coherence spectrum of $ENSO_{UEP}$ and $PDSI_{MCC}$, and **(e)** time series of $PDSI_{MCC}$. Tiles **(a)** and **(b)** also shows total variances of time series calculated with moving window of 21 years. The dark grey columns indicate periods with primary ENSO-related variance, and the light grey columns indicate periods with secondary ENSO-related variance in $PDSI_{MCC}$ (see definitions in Table 2). Tile **(e)** also shows extreme PDSI values that occurred during ENSO events. Extreme values were defined from PDSI data as 5th and 95th percentiles. PDSI data describe the hydroclimate of the March–May season.

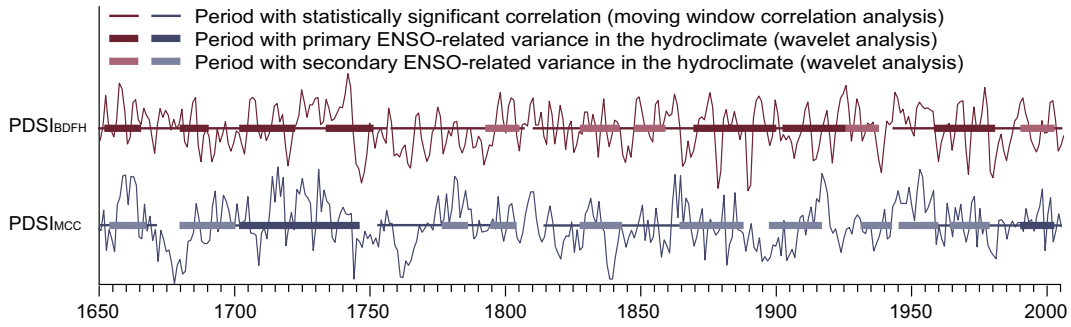

Figure 7. Periods with evidence of ENSO-related hydrological variability in March–May hydroclimate of mainland Southeast Asia over the period of 1650–2004. The periods with statistically significant correlation between the time series of $ENSO_{UEP}$ and $PDSI_{BDFH}$ and $PDSI_{MCC}$ are shown with thin horizontal lines, and the periods with primary and secondary ENSO-related variance (see definitions in Table 2) in $PDSI_{BDFH}$ and $PDSI_{MCC}$ are shown with thick horizontal lines.

MSEA during the MAM season compared to other seasons (Fig. 2). Moreover, the proxy PDSI data are most accurate for the MAM season: the tree ring data have the strongest correlation with instrumental PDSI data and provide the best verification results for the MAM season (Sano et al., 2008; Buckley et al., 2010). As argued in the Methodology section, the MAM season is also hydrologically important. For example, our analyses showed that, in the area of $PDSI_{BDFH}$, the MAM precipitation is 17 % of the annual precipitation, while for the area of $PDSI_{MCC}$ this is 22 %.

Further, the moving-window correlation was based on a window size of 21 years, resulting in ambiguity in the dating of the statistically significant periods. Third, the visual interpretation of the wavelet images involves a certain amount of subjectivity when multiple images are compared simultaneously. For example, subjective judgement was needed when the statistically significant areas in wavelet power, cross-wavelet power, and coherence spectrum images were of different size and not perfectly overlapping and when the phase arrows varied slightly from the expected direction. In order to minimise the errors from subjectivity, clear rules for consistent interpretation were developed and followed (see Sect. 2). Fourth, the size of statistically significant areas in wavelet images depended on parameters of the wavelet analysis. For example, the choice of statistical significance testing method affected the size of the statistically significant areas, which may change the timing and duration of any such identified ENSO periods with so few years. Last, it is likely that the approach used was not able to capture all individual ENSO events that resulted in hydroclimate anomalies. Despite these limitations, the results are based upon standard methods in time series analysis and are therefore considered to be reliable estimates of ENSO-related hydrological variability.

4.2 Contribution and comparison to earlier research

The past research provides a view on the general influence of ENSO on precipitation over MSEA, as discussed in the Introduction section. The El Niño (La Niña) events result in drier (wetter) conditions over MSEA (Juneng and Tangang, 2005; Kripalani and Kulkarni, 1997) and at more local scales in Thailand (Singhrattna et al., 2005b) and in the Mekong River basin (Räsänen and Kummu, 2013). These studies also suggest stronger correlation between ENSO and hydroclimate in central and southern parts of MSEA. A transition of the influence of ENSO to opposite sign from south to north is also reported for the Mekong River basin (Räsänen and Kummu, 2013) and is supported by studies focusing on the upper reaches of the Mekong and Yangtze River basins (Kiem et al., 2005; Zhang et al., 2007). The precipitation anomalies are also shown to evolve northeastward during El Niño events from southern parts of Southeast Asia to MSEA (Juneng and Tangang, 2005).

The current research confirms these past findings on the effects of ENSO on precipitation and expands the existing knowledge in three aspects: first, by providing more detailed and informative description of the seasonal evolution of the effects of ENSO in MSEA and by showing this evolution in more northern areas (compared to Juneng and Tangang, 2005) (Fig. 2); second, by showing the areas and the season when the transition of the influence of ENSO to opposite sign occurs (Fig. 2c); and third, by showing how the spatial patterns of precipitation anomalies have varied between individual ENSO events over MSEA (Fig. 3, Figs. S1 and S2). Through these contributions the current research provides a more accurate and uniform picture of the spatio-temporal effects of ENSO on precipitation and thus allows a more detailed comparison of effects of ENSO between different regions and seasons of MSEA and its largest river basins.

The long-term relationship of ENSO and hydroclimate in MSEA has been shown to exist at centennial scales by several studies (Xu et al., 2013; Buckley et al., 2007, 2010; Sano et al., 2008), but the variation of the relationship of ENSO and hydroclimate has been studied only over the past 100 years or so. Studies conducted in Thailand (Singhrattna et al., 2005b) and the Mekong River basin (Räsänen and Kummu,

Table 3. ENSO events (NOAA, 2015) and March–May precipitation anomalies in the areas of $PDSI_{BDFH}$ and $PDSI_{MCC}$ over the period of 1980–2013. Locations of PDSI areas are shown in Fig. 2. Strong ENSO events (as in NOAA, 2015) are highlighted in bold.

Year	ENSO event	Precipitation anomaly for the $PDSI_{BDFH}$ area	Precipitation anomaly for the $PDSI_{MCC}$ area
1980		−11 %	−10 %
1981		−16 %	20 %
1982	**Strong El Niño1**	**−12** %	**−12** %
1983	**Strong El Niño2**	**−41** %	**−30** %
1984		4 %	−8 %
1985		9 %	−9 %
1986	**Strong El Niño1**	**4** %	**19** %
1987	**Strong El Niño2**	**−39** %	**−27** %
1988	El Niño3/ **Strong La Niña1**	**−11** %	**4** %
1989	**Strong La Niña2**	**19** %	**6** %
1990		−7 %	18 %
1991	**Strong El Niño1**	**−23** %	**−21** %
1992	**Strong El Niño2**	**−39** %	**−50** %
1993	**Strong El Niño3**	**−14** %	**−1** %
1994	El Niño1	9 %	15 %
1995	El Niño2	−23 %	−20 %
1996		14 %	5 %
1997	**Strong El Niño1**	**10** %	**1** %
1998	**Strong El Niño2** /La Niña1	**−24** %	**−7** %
1999	La Niña2	68 %	37 %
2000	La Niña3	41 %	24 %
2001		25 %	31 %
2002	El Niño1	−19 %	15 %
2003	El Niño2	7 %	−14 %
2004		−4 %	14 %
2005		−15 %	−20 %
2006	El Niño1	8 %	5 %
2007	El Niño2/La Niña1	22 %	4 %
2008	La Niña2	31 %	17 %
2009	**Strong El Niño1**	**46** %	**3** %
2010	**Strong El Niño2/ Strong La Niña1**	**−33** %	**−30** %
2011	**Strong La Niña2**	**8** %	**15** %
2012		19 %	16 %
2013		−14 %	−7 %

2013; Räsänen et al., 2013; Darby et al., 2013) report that the most recent periods of stronger relationship between ENSO and hydroclimate occurred during the beginning of the 20th century and lasted until the 1940s, while the second period began around the 1960s–1980s.

The current research agrees with the findings from Thailand and the Mekong River basin and suggests a period of weaker relationship between ENSO and hydroclimate during the 1930s–1950s in the southern parts of the study area ($PDSI_{BDFH}$; see Figs. 1 and 7 and Table 4). The current research further expands the knowledge on the variations in ENSO's effect on the hydroclimate of MSEA in four ways. First, the research provides a view on the variation over the past 355 years: the research shows that ENSO has affected the region's hydroclimate over MAM during the majority (96 %) of the study period and during half (52 %) of the time ENSO caused significant increase in hydroclimatic variability (i.e. primary ENSO-related variance) (Fig. 7). Second, non-stationarity is revealed in the ENSO teleconnection over MSEA for the past 355 years: periods with ENSO activity and no response in the March–April hydroclimate over MSEA were observed. Third, longer-term spatial variation is shown in the effects of ENSO between individual events: the two proxy PDSI data from southern and northern MSEA responded differently to the same ENSO events and periods (Figs. 5, 6, and 7). Fourth, the research provides a quantified estimation of the occurrence of extreme dry and wet MAM seasons during ENSO events over the past 355 years. For example, in the southern parts of MSEA (areas of $PDSI_{BDFH}$), 72 % of extremely dry MAM seasons occurred during El Niño events, and 72 % of extremely wet MAM seasons occurred during La Niña events. Altogether the long-term analyses improve the understanding of the ENSO teleconnection and its variability over MSEA for the 3.5 centuries.

It is worthwhile to further highlight that the article's demonstration of the strong inverse relationship between the reconstructed drought metric PDSI and ENSO fit within a broader context of studies demonstrating the importance of ENSO. The tree ring studies used here (Sano et al., 2008; Buckley et al., 2010) focus on northern and southern Vietnam. Buckley et al. (2014) expand upon this discussion by using tree ring records from all across monsoon Asia and North America, illustrating that the dominant mode of climate variability across both sides of the Pacific is driven by ENSO-like variability, particularly at decadal scales (i.e. the Interdecadal Pacific Oscillation, or IPO – see Meehl and Hu (2006) and Buckley et al. (2010) for further details). Indeed, other tree ring sites from Thailand (Buckley et al., 2007) and Myanmar (D'Arrigo et al., 2011) confirm the strength of this relationship in these regions as well.

4.3 Future research directions and implications for adaptation

The findings of the current paper indicate considerable uncertainties in the effects of ENSO on hydroclimate and how this relationship develops through time. For example, clear patterns were found in the seasonal evolution of precipitation anomalies during ENSO events, but at the same time the precipitation anomalies and their spatio-temporal patterns were found to vary considerably between ENSO events. This leads to two potentially useful research directions related to ENSO. The first research direction would explore the physical characteristics (e.g. sea surface temperature, air pressure, wind, and moisture fluxes patterns) of each ENSO event and how they translate into anomalies of MSEA hydroclimate. For example, it is hypothesised that the placement of the descending limb of the Walker circulation could affect the ENSO

Table 4. Periods with evidence of ENSO teleconnection in March–May hydroclimate of mainland Southeast Asia over the period of 1650–2004. "Correlation periods" refer to periods with statistically significant correlation in moving-window correlation analysis (Fig. 4), and "periods with primary and secondary ENSO-related variance in hydroclimate" refer to periods when ENSO had stronger influence on hydroclimate according to wavelet analyses (Figs. 5–6). Statistically significant periods ($p < 0.05$) are in bold.

Correlation periods			Periods with primary and secondary ENSO-related variance in hydroclimate			Evidence of ENSO teleconnection mainland Southeast Asia
$PDSI_{BDFH}$	$PDSI_{MCC}$	Combined	$PDSI_{BDFH}$	$PDSI_{MCC}$	Combined	
1667–1765	**1663–1684**	**1663–1814**	**1653–1644**	1655–1666	1653–1666	1663–1814
1767–1814	**1696–1716**	**1817–1940**	**1681–1689**	1681–1699	1681–1699	1817–2004
1817–1839	**1724–1752**	**1943–2004**	**1703–1721**	**1703–1745**	1703–1750	
1842–1940	**1762–1811**		**1735–1750**	1778–1785	1778–1785	
1943–2004	**1821–1884**		1794–1804	1796–1803	1794–1804	
	1949–2004		1829–1841	1829–1842	1829–1842	
			1849–1858	1866–1887	1849–1858	
			1871–1899	1899–1918	1866–1942	
			1904–1925	1933–1942	1947–1980	
			1926–1937	1947–1959	1992–2002	
			1960–1980	1966–1978		
			1992–2002	**1992–2002**		

teleconnection over MSEA (Singhrattna et al., 2005b). The second direction could be to explore how other climatic and oceanic phenomena interact with the ENSO teleconnection over MSEA. For example, it is known that the Indian Ocean Dipole (IOD) affects the hydroclimate over MSEA (Darby et al., 2013), and there are good indications of the effect of the Pacific Decadal Oscillation (PDO) (Delgado et al., 2012). In addition, the current research discovered statistically significant positive correlation between precipitation and MEI_{JFM} in the northern regions of MSEA during the DJF (0/1) season but did not investigate it further. To our knowledge this phenomenon has not been investigated before and therefore calls for further research.

The findings of this study also provide perspectives for adaptation to extremes in hydroclimate. The findings suggest some degree of statistical predictability of ENSO-related anomalies in hydroclimate, but at the same time the findings revealed large variation and thus uncertainties in the effects of ENSO over MSEA. It is well known that statistical approaches can have limitations when it comes to predicting extreme events (see e.g. Nassim, 2010). Thus, given the high variability in the effects of ENSO, limitations in the current knowledge, and statistical approaches we suggest exploration of adaptation approaches that embrace uncertainty and complexity and seek adaptation opportunities in multiple sectors and levels of society (see e.g. Resilience concept: Walker et al., 2004, 2013) while considering ongoing anthropogenic environmental changes (Keskinen et al., 2010; Lauri et al., 2012; Pech and Sunada, 2008). For example, adaptation only through engineering solutions is likely to aggravate already-existing challenges (e.g. Baran and Myschowoda, 2009). The suggested adaptation approaches could further benefit from analysis of the societal impacts of the identified historical events and the coping mechanisms used to deal with them in the past (Nuorteva et al., 2010; Buckley et al., 2010).

5 Conclusions

Hydroclimate variability affects various economic activities, local livelihoods, and food security across MSEA. This research sought to improve our understanding of the hydroclimate variability by investigating the spatial and temporal variability of MSEA's ENSO over the period of 1650–2013. The investigations were based on analyses of gridded seasonal precipitation data (1980–2013), proxy Palmer drought severity index values for the March–May season, and proxy ENSO data (1650–2004).

These analyses provide a more accurate and uniform picture of the spatio-temporal effects of ENSO on precipitation and improve our understanding of the long-term ENSO teleconnection and its variability over MSEA. The research reveals new information on the seasonal evolution of the effects of ENSO over MSEA, and it shows how the spatial patterns of the effects of ENSO vary between individual events. On a longer timescale, the strength of the effects of ENSO on hydroclimate of the March–April season (the important monsoon transition season with most-widespread ENSO effects in MSEA) was shown to vary between periods of weaker and stronger effects. Altogether our findings reinforce the significance of ENSO over MSEA, but they also expand the past knowledge by describing the high degree of variability and non-stationarity in the effects of ENSO. This described variability implies challenges for understanding and predicting the effects of ENSO over MSEA into the future.

Given the high impact and variability of ENSO, and limitations in the current knowledge and predictive skill, adaptive

approaches for mitigating the negative effects of ENSO are recommended. Adaptation should embrace uncertainty, seek adaptation opportunities within multiple sectors and levels of society, and consider climate-related adaptation as part of broader adaptation to ongoing social and environmental changes. Forecasting- and engineering-based approaches alone are likely to be inadequate and will risk creating further challenges.

6 Data availability

All data used in this study is publicly available. The precipitation data (GPCC v.7; Schneider et al., 2015) are is available at Deutscher Wetterdienst: doi:10.5676/DWD_GPCC/FD_M_V7_050; the multivariate ENSO index (Wolter and Timlin, 1993, 1998) is available at National Oceanic and Air Administration's (NOAA) Earth System Research Laboratory: http://www.esrl.noaa.gov/psd/enso/mei; the unified ENSO proxy (McGregor et al., 2010) is available at National Oceanic and Air Administration's (NOAA) National Climatic Data Center (NCDC): https://www.ncdc.noaa.gov/paleo/study/8732; the multi-proxy ENSO event reconstruction (Gergis and Fowler, 2009) is available at NOAA's NCDC: https://www.ncdc.noaa.gov/paleo/study/8408; and the PDSI proxies (Sano et al., 2008; Buckley et al., 2010) can be extracted from Monsoon Asia Drought Atlas (Cook et al., 2010) which can be downloaded from NOAA's NCDC: http://www.ncdc.noaa.gov/paleo/pubs/cook2010/cook2010.html.

The Supplement related to this article is available online at doi:10.5194/cp-12-1889-2016-supplement.

Acknowledgements. Timo A. Räsänen and Ville Lindgren received funding from Maa- ja vesitekniikan tuki ry, Joseph H. A. Guillaume from the Academy of Finland-funded project NexusAsia (grant no. 269901), Brendan. M. Buckley from NSF grants GEO 09-08971 and AGS 130-3976, and Matti Kummu from the Academy of Finland-funded project SCART (267463) and the Emil Aaltonen Foundation-funded project "eat-less-water". Lamont contribution number 8055.

Edited by: D. Fleitmann
Reviewed by: two anonymous referees

References

Adamson, P. and Bird, J.: The Mekong: A Drought-prone Tropical Environment?, Int. J. Water Resour. D., 26, 579–594, doi:10.1080/07900627.2010.519632, 2010.

ADB: GMS Statistics, Asian Development Bank, Greater Mekong Subregion Core Environment Program, available at: http://www.gms-eoc.org, last access: 13 September 2016.

Anchukaitis, K. J., Cook, B. I., Cook, E. R., Buckley, B. M., and Fa, Z.-X.: Mekong River flow reconstructed from tree rings, Geophys. Res. Lett., in review, 2016.

Baran, E. and Myschowoda, C.: Dams and fisheries in the Mekong Basin, Aquat. Ecosyst. Health, 12, 227–234, 2009.

Buckley, B., Palakit, K., Duangsathaporn, K., Sanguantham, P., and Prasomsin, P.: Decadal scale droughts over northwestern Thailand over the past 448 years: links to the tropical Pacific and Indian Ocean sectors, Clim. Dynam., 29, 63–71, 2007.

Buckley, B. M., Anchukaitis, K. J., Penny, D., Fletcher, R., Cook, E. R., Sano, M., Nam, L. C., Wichienkeeo, A., Minh, T. T., and Hong, T. M.: Climate as a contributing factor in the demise of Angkor, Cambodia, P. Natl. Acad. Sci. USA, 107, 6748–6752, doi:10.1073/pnas.0910827107, 2010 (data available at: http://www.ncdc.noaa.gov/paleo/pubs/cook2010/cook2010.html).

Buckley, B. M., Fletcher, R., Wang, S.-Y. S., Zottoli, B., and Pottier, C.: Monsoon extremes and society over the past millennium on mainland Southeast Asia, Quaternary Sci. Rev., 95, 1–19, doi:10.1016/j.quascirev.2014.04.022, 2014.

Cai, W., Borlace, S., Lengaigne, M., van Rensch, P., Collins, M., Vecchi, G., Timmermann, A., Santoso, A., McPhaden, M. J., Wu, L., England, M. H., Wang, G., Guilyardi, E., and Jin, F.-F.: Increasing frequency of extreme El Niño events due to greenhouse warming, Nature Climate Change, 4, 111–116, 2014.

Cane, M. A.: The evolution of El Niño, past and future, Earth Planet. Sc. Lett., 230, 227–240, 2005.

Cook, B. I., Bell, A. R., Anchukaitis, K. J., and Buckley, B. M.: Snow cover and precipitation impacts on dry season streamflow in the Lower Mekong Basin, J. Geophys. Res.-Atmos., 117, D16116, doi:10.1029/2012JD017708, 2012.

Cook, E. R., Anchukaitis, K. J., Buckley, B. M., D'Arrigo, R. D., Jacoby, G. C., and Wright, W. E.: Asian Monsoon Failure and Megadrought During the Last Millennium, Science, 328, 486–489, doi:10.1126/science.1185188, 2010.

Dai, A., Trenberth, K. E., and Qian, T.: A Global Dataset of Palmer Drought Severity Index for 1870–2002: Relationship with Soil Moisture and Effects of Surface Warming, J. Hydrometeorol., 7, 1117–1130, 2004.

Darby, S. E., Leyland, J., Kummu, M., Räsänen, T. A., and Lauri, H.: Decoding the drivers of bank erosion on the Mekong river: The roles of the Asian monsoon, tropical storms, and snowmelt, Water Resour Res., 49, 1–18, 2013.

D'Arrigo, R., Palmer, J., Ummenhofer, C. C., Kyaw, N. N., and Krusic, P.: Three centuries of Myanmar monsoon climate variability inferred from teak tree rings, Geophys. Res. Lett., 38, L24705, doi:10.1029/2011GL049927, 2011.

Delgado, J. M., Merz, B., and Apel, H.: A climate-flood link for the lower Mekong River, Hydrol. Earth Syst. Sci., 16, 1533–1541, doi:10.5194/hess-16-1533-2012, 2012.

Fukai, S., Sittisuang, P., and Chanphengsay, M.: Increasing Production of Rainfed Lowland Rice in Drought Prone Environments, Plant Production Sci., 1, 75–82, doi:10.1626/pps.1.75, 1998.

Gergis, J. L. and Fowler, A. M.: A history of ENSO events since A.D. 1525: implications for future climate change, Climatic Change, 92, 343–387, doi:10.1007/s10584-008-9476-z,

2009 (data available at: https://www.ncdc.noaa.gov/paleo/study/8408).

Grinsted, A., Moore, J. C., and Jevrejeva, S.: Application of the cross wavelet transform and wavelet coherence to geophysical time series, Nonlin. Processes Geophys., 11, 561–566, doi:10.5194/npg-11-561-2004, 2004.

Harris, I., Jones, P. D., Osborn, T. J., and Lister, D. H.: Updated high-resolution grids of monthly climatic observations – the CRU TS3.10 Dataset, Int. J. Climatol., 34, 623–642, doi:10.1002/joc.3711, 2014.

Hsu, H.-H., Zhou, T., and Matsumoto, J.: East Asian, Indochina and Western North Pacific Summer Monsoon – An update, Asia-Pacific J. Atmos. Sci., 50, 45–68, doi:10.1007/s13143-014-0027-4, 2014.

Juneng, L. and Tangang, F.: Evolution of ENSO-related rainfall anomalies in Southeast Asia region and its relationship with atmosphere–ocean variations in Indo-Pacific sector, Clim. Dynam., 25, 337–350, 2005.

Keskinen, M., Chinvanno, S., Kummu, M., Nuorteva, P., Snidvongs, A., Varis, O., and Västilä, K.: Climate change and water resources in the Lower Mekong River Basin: putting adaptation into the context, Journal of Water and Climate Change, 1, 103–117, doi:10.2166/wcc.2010.009, 2010.

Kiem, A., Geogievsky, M., Hapuarachchi, H., Ishidaira, H., and Takeuchi, K.: Relationship between ENSO and snow covered area in the Mekong and Yellow river basins in: Proceedings of symposium S6, Proceedings of symposium S6 held in 7th IAHS Scientific Assembly, Foz do Iguacu, Brazil, 2005.

Kripalani, R. H. and Kulkarni, A.: Rainfall variability over South-East Asia – Connections with Indian Monsoon and ENSO extremes: New perspectives, Int. J. Climatol., 17, 1155–1168, 1997.

Lauri, H., de Moel, H., Ward, P. J., Räsänen, T. A., Keskinen, M., and Kummu, M.: Future changes in Mekong River hydrology: impact of climate change and reservoir operation on discharge, Hydrol. Earth Syst. Sci., 16, 4603–4619, doi:10.5194/hess-16-4603-2012, 2012.

McGregor, S., Timmermann, A., and Timm, O.: A unified proxy for ENSO and PDO variability since 1650, Clim. Past, 6, 1–17, doi:10.5194/cp-6-1-2010, 2010 (data available at: https://www.ncdc.noaa.gov/paleo/study/8732).

McGregor, S., Timmermann, A., England, M. H., Elison Timm, O., and Wittenberg, A. T.: Inferred changes in El Niño-Southern Oscillation variance over the past six centuries, Clim. Past, 9, 2269–2284, doi:10.5194/cp-9-2269-2013, 2013.

Meehl, G. A. and Hu, A.: Megadroughts in the Indian Monsoon Region and Southwest North America and a Mechanism for Associated Multidecadal Pacific Sea Surface Temperature Anomalies, J. Climate, 19, 1605–1623, doi:10.1175/JCLI3675.1, 2006.

MRC: State of the Basin Report 2010, Mekong River Commission, Vientiane, Lao PDR, available at: http://www.mrcmekong.org/assets/Publications/basin-reports/MRC-SOB-report-2010full-report.pdf (last access: June 2012), 2010.

Nassim, N. T.: The black swan: the impact of the highly improbable, Second Edn., Random House Inc., New York, 2010.

NOAA: Multivariate ENSO Index, National Oceanic and Atmospheric Administration, Earth System Research Laboratory, available at: http://www.esrl.noaa.gov/psd/enso/mei/, last access: July 2015.

Nuorteva, P., Keskinen, M., and Varis, O.: Water, livelihoods and climate change adaptation in the Tonle Sap Lake area, Cambodia: learning from the past to understand the future, Journal of Water and Climate Change, 1, 87–101, doi:10.2166/wcc.2010.010, 2010.

Palmer, W. C.: Meteorological drought, US Weather Bureau, Washington D.C., 58, 1965.

Pech, S. and Sunada, K.: Population Growth and Natural-Resources Pressures in the Mekong River Basin, AMBIO, 37, 219–224, 2008.

Räsänen, T. A. and Kummu, M.: Spatiotemporal influences of ENSO on precipitation and flood pulse in the Mekong River Basin, J. Hydrol., 476, 154–168, 2013.

Räsänen, T. A., Lehr, C., Mellin, I., Ward, P. J., and Kummu, M.: Palaeoclimatological perspective on river basin hydrometeorology: case of the Mekong Basin, Hydrol. Earth Syst. Sci., 17, 2069–2081, doi:10.5194/hess-17-2069-2013, 2013.

Rösch, A. and Schmidbauer, H.: WaveletComp: A guided tour through the R-package, 2014, available at: http://www.hs-stat.com/projects/WaveletComp/WaveletComp_guided_tour.pdf, last access: 13 September 2016.

Sano, M., Buckley, B., and Sweda, T.: Tree-ring based hydroclimate reconstruction over northern Vietnam from Fokienia hodginsii: eighteenth century mega-drought and tropical Pacific influence, Clim. Dynam., 33, 331–340, 2008 (data available at: http://www.ncdc.noaa.gov/paleo/pubs/cook2010/cook2010.html).

Sawano, S., Hasegawa, T., Goto, S., Konghakote, P., Polthanee, A., Ishigooka, Y., Kuwagata, T., and Toritani, H.: Modeling the dependence of the crop calendar for rain-fed rice on precipitation in Northeast Thailand, Paddy and Water Environment, 6, 83–90, doi:10.1007/s10333-007-0102-x, 2008.

Schneider, U., Becker, A., Finger, P., Meyer-Christoffer, A., Rudolf, B., and Ziese, M.: GPCC Full Data Reanalysis Version 7.0 at 0.5°: Monthly Land-Surface Precipitation from Rain-Gauges built on GTS-based and Historic Data, doi:10.5676/DWD_GPCC/FD_M_V7_050, 2015.

Singhrattna, N., Rajagopalan, B., Clark, M., and Krishna Kumar, K.: Seasonal forecasting of Thailand summer monsoon rainfall, Int. J. Climatol., 25, 649–664, 2005a.

Singhrattna, N., Rajagopalan, B., Kumar, K. K., and Clark, M.: Interannual and Interdecadal Variability of Thailand Summer Monsoon Season, J. Climate, 18, 1697–1708, 2005b.

Torrence, C. and Compo, G. P.: A practical guide to wavelet analysis, B. Am. Meteorol. Soc., 79, 61–78, 1998.

Trenberth, K. E. and Shea, D. J.: On the Evolution of the Southern Oscillation, Mon. Weather Rev., 115, 3078–3096, doi:10.1175/1520-0493(1987)115<3078:OTEOTS>2.0.CO;2, 1987.

Walker, B., Holling, C. S., Carpenter, S. R., and Kinzig, A. P.: Resilience, Adaptability and Transformability in Social–ecological Systems, Ecol. Soc., 9, doi:10.1175/1520-0493(1987)115<3078:OTEOTS>2.0.CO;2, 2004.

Walker, W. E., Haasnoot, M., and Kwakkel, J.: Adapt or Perish: A Review of Planning Approaches for Adaptation under Deep Uncertainty, Sustainability, 5, 955–979, doi:10.3390/su5030955, 2013.

Wang, B., Yang, J., Zhou, T., and Wang, B.: Inter-decadal Changes in the Major Modes of Asian-Australian Monsoon Variability:

Strengthening Relationship with ENSO since the Late 1970s*, J. Climate, 21, 1771–1789, 2008.

Ward, P. J., Eisner, S., Flörke, M., Dettinger, M. D., and Kummu, M.: Annual flood sensitivities to El Niño-Southern Oscillation at the global scale, Hydrol. Earth Syst. Sci., 18, 47–66, doi:10.5194/hess-18-47-2014, 2014.

Wolter, K. and Timlin, M. S.: Monitoring ENSO in COADS with a seasonally adjusted principal component index, Proc. of the 17th Climate Diagnostics Workshop, Norman, OK, NOAA/NMC/CAC, NSSL, Oklahoma Clim. Survey, CIMMS and the School of Meteor., University of Oklahoma, 52–57, 1993 (data available at: http://www.esrl.noaa.gov/psd/enso/mei).

Wolter, K. and Timlin, M. S.: Measuring the strength of ENSO events – how does 1997/98 rank?, Weather, 53, 315–324, 1998 (data available at: http://www.esrl.noaa.gov/psd/enso/mei).

Xu, C., Sano, M., and Nakatsuka, T.: A 400-year record of hydroclimate variability and local ENSO history in northern Southeast Asia inferred from tree-ring δ^{18}O, Palaeogeogr. Palaeocl., 386, 588–598, doi:10.1016/j.palaeo.2013.06.025, 2013.

Yatagai, A., Arakawa, O., Kamiguchi, K., Kawamoto, H., Nodzu, M., and Hamada, A.: A 44-year daily gridded precipitation dataset for Asia based on a dense network of rain gauges, SOLA, 5, 137–140, doi:10.2151/sola.2009-035, 2009.

Yatagai, A., Kamiguchi, Arakawa, O., Hamada, A., Yasutomi, N., and Kitoh, A.: APHRODITE: Constructing a long-term daily gridded precipitation dataset for Asia based on a dense network of rain gauges, B. Am. Meteorol. Soc., 93, 1401–1415, doi:10.1175/BAMS-D-11-00122.1, 2012.

Zhang, Q., Xu, C.-Y., Jiang, T., and Wu, Y.: Possible influence of ENSO on annual maximum streamflow of the Yangtze River, China, J. Hydrol., 333, 265–274, 2007.